crystals

MDPI

Article

Synthesis of $NiCo_2S_4$@$NiMoO_4$ Nanosheets with Excellent Electrochemical Performance for Supercapacitor

Jian Wang [1,2,3,*], Yucai Li [1,2,3], Yan Zhao [1,2,3], Dong Zhang [1,2,3], Shiwei Song [1,2,3] and Junjie Ke [1,2]

1 School of Renewable Energy, Shenyang Institute of Engineering, Shenyang 110136, China
2 Liaoning Engineering Research Center of Renewable Energy Photoelectric Material Preparation and Analysis, Shenyang Institute of Engineering, Shenyang 110136, China
3 Liaoning Key Laboratory of Regional Multi-Energy System Integration and Control, Shenyang Institute of Engineering, Shenyang 110136, China
* Correspondence: wangjian_shm@163.com

Abstract: Currently, the research of energy storage devices mainly focuses on enhancing their electrochemical performance. Core-shell structured $NiCo_2S_4$@$NiMoO_4$ is thought to be one of the most promising electrode materials for supercapacitors due to its high specific capacitance and excellent cycle performance. In this work, we report $NiCo_2S_4$@$NiMoO_4$ nanosheets on Ni foam by a two-step fabricated method. The as-obtained product has a high capacitance of 1035 F g^{-1} at 1 A g^{-1}. The as-assembled supercapacitor has a high energy density of 32.4 W h kg^{-1} at a power density of 3230 W kg^{-1} and a superior cycle performance, with 70.1% capacitance retention. The electrode materials reported here might exhibit potential applications in future energy storage devices.

Keywords: $NiCo_2S_4$@$NiMoO_4$; electrochemical performance; battery-type electrode; asymmetric supercapacitor; cyclic stability

Citation: Wang, J.; Li, Y.; Zhao, Y.; Zhang, D.; Song, S.; Ke, J. Synthesis of $NiCo_2S_4$@$NiMoO_4$ Nanosheets with Excellent Electrochemical Performance for Supercapacitor. *Crystals* **2022**, *12*, 821. https://doi.org/10.3390/cryst12060821

Academic Editor: Sergio Brutti

Received: 7 May 2022
Accepted: 7 June 2022
Published: 10 June 2022

1. Introduction

In today's highly developed society, the demand for energy has reached a supreme point. With the shortage of fossil energy, the call to develop clean energy is increasing day by day. Thus, it is urgent to design and develop sustainable devices for energy storage and conversion [1–4]. Among all kinds of energy storage equipment, supercapacitors are widely acknowledged for their fast charge–discharge rate, high power density, long cycling life and environmentally benign behavior [5,6]. However, the low energy density of supercapacitors limits their further application in the field of energy storage. According to the different charge storage mechanisms, supercapacitor electrodes can be classified into electric double layer electrodes and pseudo-capacitors [7,8]. The energy storage of pseudocapacitive electrode materials mainly depends on Faraday redox reaction, which makes the specific capacitance and energy density of pseudocapacitive electrodes higher than that of EDLEs [9–11]. The materials of pseudo-capacitors mainly include transition metal oxides, nitrides, sulfides and conducting polymers.

Transition metal compounds have been proved to be reliable electrode materials for supercapacitors, which have better electron conductivity and cycling stability than metal oxides [12,13]. Among them, $NiCo_2S_4$ is considered to be one of the most promising electrode materials for supercapacitors because of its unique atomic structure and electronic properties [14,15]. In particular, $NiMoO_4$ is provided with high theoretical capacity, excellent rate performance, good conductivity and high redox reversibility. However, cycle performance and specific capacitance usually restricts their electrochemical performance. In order to deal with above issues, Various nanostructures of $NiCo_2S_4$/$NiMoO_4$ nanostructures, such as nanorods, nanosheet arrays, nanoneedle-sheets and core-shell structures have been explored as electrode materials for supercapacitors, and have been proved to have excellent electrochemical properties [16–18]. This is because the single-electrode materials are limited

by their slow reaction kinetics, moderate active sites, unstable structure, poor cycle stability and low rate performance [19]. At the same time, the low energy density severely limits the large-scale application of its devices. Therefore, it is still a great challenge to design and prepare structurally stable $NiCo_2S_4$@$NiMoO_4$ electrode materials.

Herein, we synthesized $NiCo_2S_4$@$NiMoO_4$ samples using the two-step method. The nanosheet structure provides a shorter transport path for ions and electrons. The $NiCo_2S_4$@$NiMoO_4$ nanosheets as supercapacitor electrode materials show high capacitance of 1035 F g^{-1} at a current density of 1 A g^{-1} and good capacitive retention after 10,000 cycles. Moreover, an asymmetric supercapacitor is constructed by $NiCo_2S_4$@$NiMoO_4$ structures as positive electrode and active carbon as negative electrode. It possesses an energy density of 32.4 W h kg^{-1} at a power density of 3230 W kg^{-1}. These excellent electrochemical performances could be credited to its unique nanosheets structure.

2. Experimental

2.1. Synthesis of $NiCo_2S_4$@$NiMoO_4$ Structure

At first, $NiCo_2S_4$ nanosheets were grown on Ni foam by a simple solvothermal method. A total of 1 mM $NiCl_2 \cdot 6H_2O$, 2 mM $CoCl_2 \cdot 6H_2O$, 1.0 g Urea and 0.6 g NH_4F were dissolved in 40 mL solution of deionized water and stirred for 30 min under constant magnetic force. Then, the above solution with the pretreated Ni foam was transferred into an 80 mL autoclave and kept at 100 °C for 8 h. After natural cooling down to room temperature, the as-synthesized samples were taken out and washed with deionized water. $NiCo_2S_4$ was prepared through a vulcanization process. A total of 0.3 g Na_2S was added into 50 mL DI water and the above obtained samples were added into 80 mL autoclave and kept at 120 °C for 4 h.

Hybrid $NiCo_2S_4$@$NiMoO_4$ structures were fabricated by a subsequently hydrothermal method; 0.5 mM $NiCl_2 \cdot 6H_2O$, 0.5 mM $NaMoO_4$, 0.6 g Urea and 0.3 g NH_4F were dissolved in 40 mL solution of deionized water and carried out at 160 °C for 6 h. The average mass loads were 1.3 and 1.7 mg cm^{-2}, respectively.

2.2. Electrochemical Measurements

The electrochemical properties of the synthesized products are tested by chi660e electrochemical workstation (Shanghai Chenhua, China). During the testing procedure, the Pt foil and Hg/HgO electrode were used for the purpose of the counter and reference electrodes, respectively. Moreover, the $NiCo_2S_4$@$NiMoO_4$ product was used as a working electrode. Cyclic voltammetry curves (CV), galvanostatic charge–discharge (GCD) and electrochemical impedance spectroscopy (EIS) measurements were measured in a 3 M KOH aqueous electrolyte.

2.3. Assembly of the Asymmetric Supercapacitor

All-solid-state supercapacitors were manufactured by using $NiCo_2S_4$@$NiMoO_4$ and AC (active carbon) as cathode and anode respectively, and using a separator and PVA-KOH gel as polymer electrolyte. AC electrode was fabricated by mixing AC, carbon black and 7 wt% polymer binders (polyvinylidene fluoride, PVDF) in a weight ratio of 7:2:1.

3. Results and Discussion

Firstly, crystalline structure and phase purity of the products are analyzed by XRD. Figure 1 shows the XRD spectra of the samples as-prepared samples. The three samples have sharp diffraction peaks at 2 theta value of 44.5°, 51.8° and 76.4°, corresponding to the surface index (111), (200) and (220) of Ni foam. It is found that there are several distinct diffraction peaks at 21.8°, 31.1°, 37.8°, 50.1° and 55.2° corresponding to (101), (110), (003), (211) and (122) crystal planes of $NiCo_2S_4$ (JCPDS No.20-0782), respectively. Other peaks at 21.8°, 31.1°, 37.8°, 50.1° and 55.2° corresponding to (101), (110), (003), (211) and (122) crystal planes, respectively, can be indexed to $NiMoO_4$ (JCPDS No.12-0348). There is no

diffraction peak of other impurities, which indicates that the sample is $NiCo_2S_4$@$NiMoO_4$ phase with high purity.

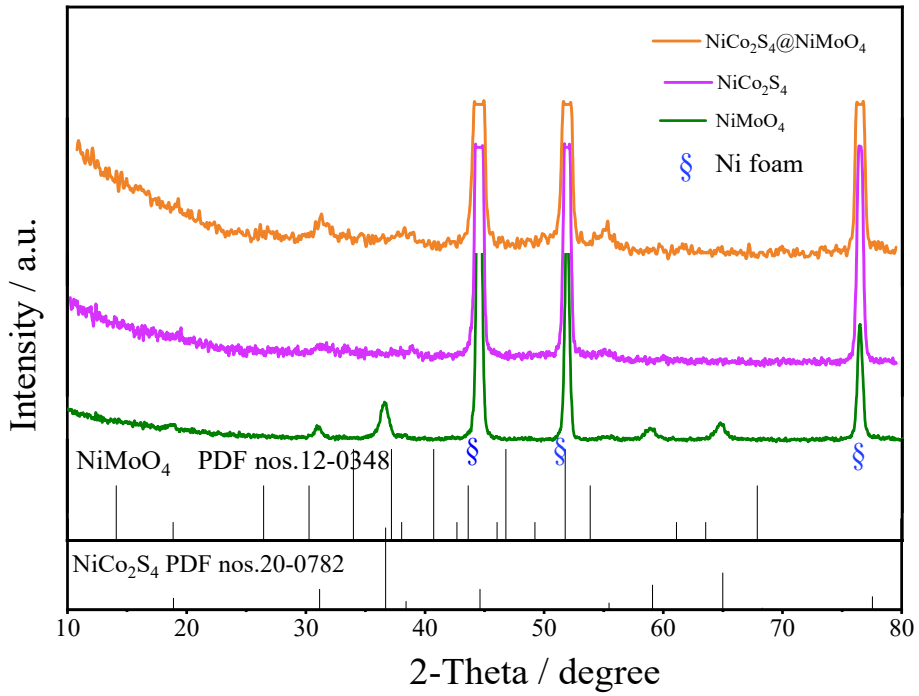

Figure 1. Structure characterization for XRD pattern of the samples.

Figure 2a shows Co 2p spectra, two distinct characteristic peaks at the binding energy of 777.8 eV and 795.1 eV, which are consistent with Co $2p_{3/2}$ and Co $2p_{1/2}$, respectively [20]. The existence of Co^{2+} and Co^{3+} can be proved by spin orbit coupling. In addition, the satellite peaks at the binding energies of 784.8 eV and 879.2 eV are named Sat., which are caused by the electronic transition in the valence band [21,22]. Mo 3d spectra are shown in Figure 2b. $NiCo_2O_4$@$NiMoO_4$ samples exhibit two peaks at 229.9 and 232.5 eV, which correspond to Mo $3d_{5/2}$ and Mo $3d_{3/2}$. Binding energy at 235.23, 230.4 and 226.5 eV corresponds to Mo-S bond [23,24]. Ni 2p emission spectra are fitted with two kinds of nickel species containing Ni^{2+} and Ni^{3+} (Figure 2c). Binding energies at 853.4 eV and 856.5 eV correspond to Ni $2p_{3/2}$ and those at 874.5 and 871.6 eV for Ni $2p_{1/2}$. Those at 787 and 873 eV could be indexed to shakeup satellites (noted as Sat.), revealing that most of Ni exists in the form of Ni^{2+} ion [25,26]. The S 2p spectrum in Figure 2d shows two characteristic peaks at 162.59 eV and 163.2 eV, which can be ascribed to S $2p_{1/2}$ and S $2p_{3/2}$, respectively, indicating that the S^{2+} valence exists in $NiCo_2S_4$@$NiMoO_4$. Furthermore, a satellite peak of S was checked at 168.2 eV [27], which may be owing to the high oxidation of S on the surface of $NiCo_2S_4$@$NiMoO_4$ sample during the test procedure. XPS characterization further proved that the prepared $NiCo_2S_4$@$NiMoO_4$ sample had high purity and good crystal quality [28].

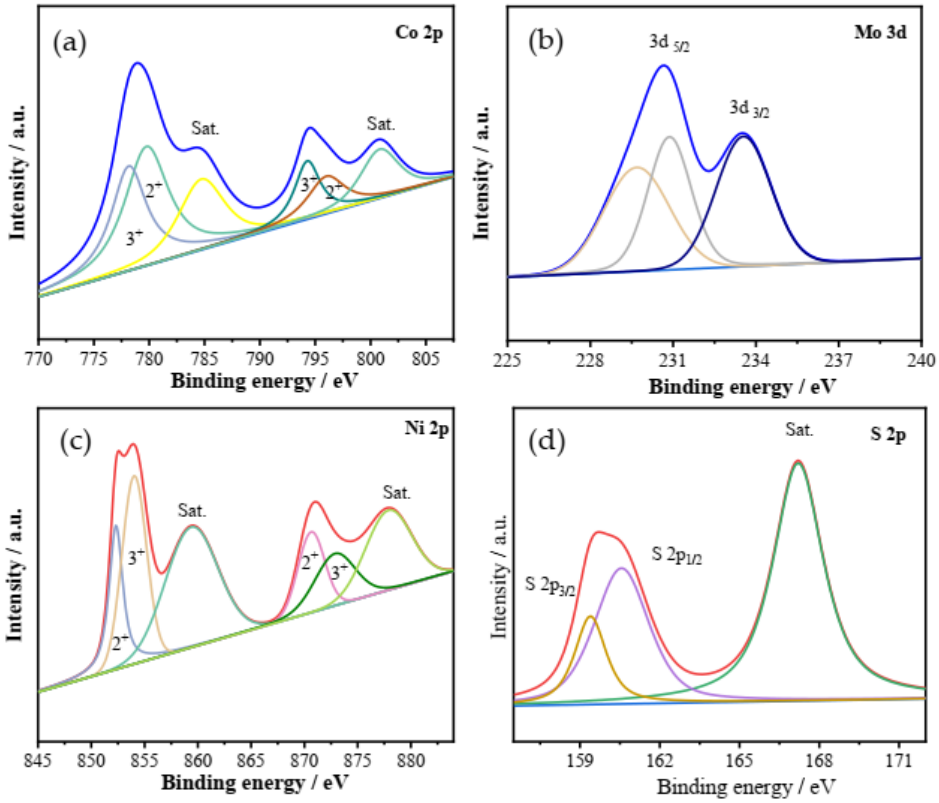

Figure 2. (**a**) XPS of Co 2p of the $NiCo_2S_4$@$NiMoO_4$ samples (**b**) Mo 3d of the $NiCo_2S_4$@$NiMoO_4$ samples (**c**) Ni 2p of the $NiCo_2S_4$@$NiMoO_4$ samples (**d**) S 2p of the $NiCo_2S_4$@$NiMoO_4$ samples.

SEM and TEM were used to analyze the surface morphology and structure of as-prepared products. Figure 3a,b shows the SEM images of the prepared products at different magnification. Ni foam surface is covered with a three-dimensional nanowires structures (Figure 3a). From high magnification SEM images (Figure 3b), it is found that adjacent nanowires are linked to each other. Figure 3c,d show SEM images of hybrid $NiCo_2S_4$@$NiMoO_4$ samples. The diameter of the nanowires is 30 nm. From the TEM images of Figure 3e, a layer of nanosheets uniformly coat on the surface of $NiCo_2S_4$ nanosheest, which exhibited fill consistency with the observed SEM images. The HRTEM image of Figure 3f shows that the lattice distances of 0.281 and 0.288 nm correspond to the (311) and (111) faces of $NiCo_2S_4$ and $NiMoO_4$, respectively.

Figure 4a–c shows the CV curve of $NiCo_2S_4$@$NiMoO_4$, $NiCo_2S_4$ and $NiMoO_4$ electrodes at different scan rates. At different scanning rates, there are obvious oxidation and reduction peaks, which are caused by the reversible redox reaction. With the increase of scanning rate, the positions of oxidation peak and reduction peak move to positive voltage and negative voltage, respectively, and the CV curve still keeps a similar shape and the envelope area becomes larger, which proves that $NiCo_2S_4$@$NiMoO_4$ electrode has the characteristics of fast charge–discharge and high-rate capacity. Figure 4d–f shows the GCD curves of $NiCo_2S_4$@$NiMoO_4$, $NiCo_2S_4$ and $NiMoO_4$ electrodes between 0 and 0.5 V at different current densities. It can be observed that these curves are symmetrical, and each curve shows a relatively flat area, which reveals the Faraday characteristics of the electrode material and high reversibility of its Faraday reaction. In addition, the capacitance of $NiCo_2S_4$@$NiMoO_4$-8 electrode is 1035, 805, 613, 374 and 198 F g^{-1} at the current densities of 1, 2, 4, 6 and 8 A g^{-1}, respectively.

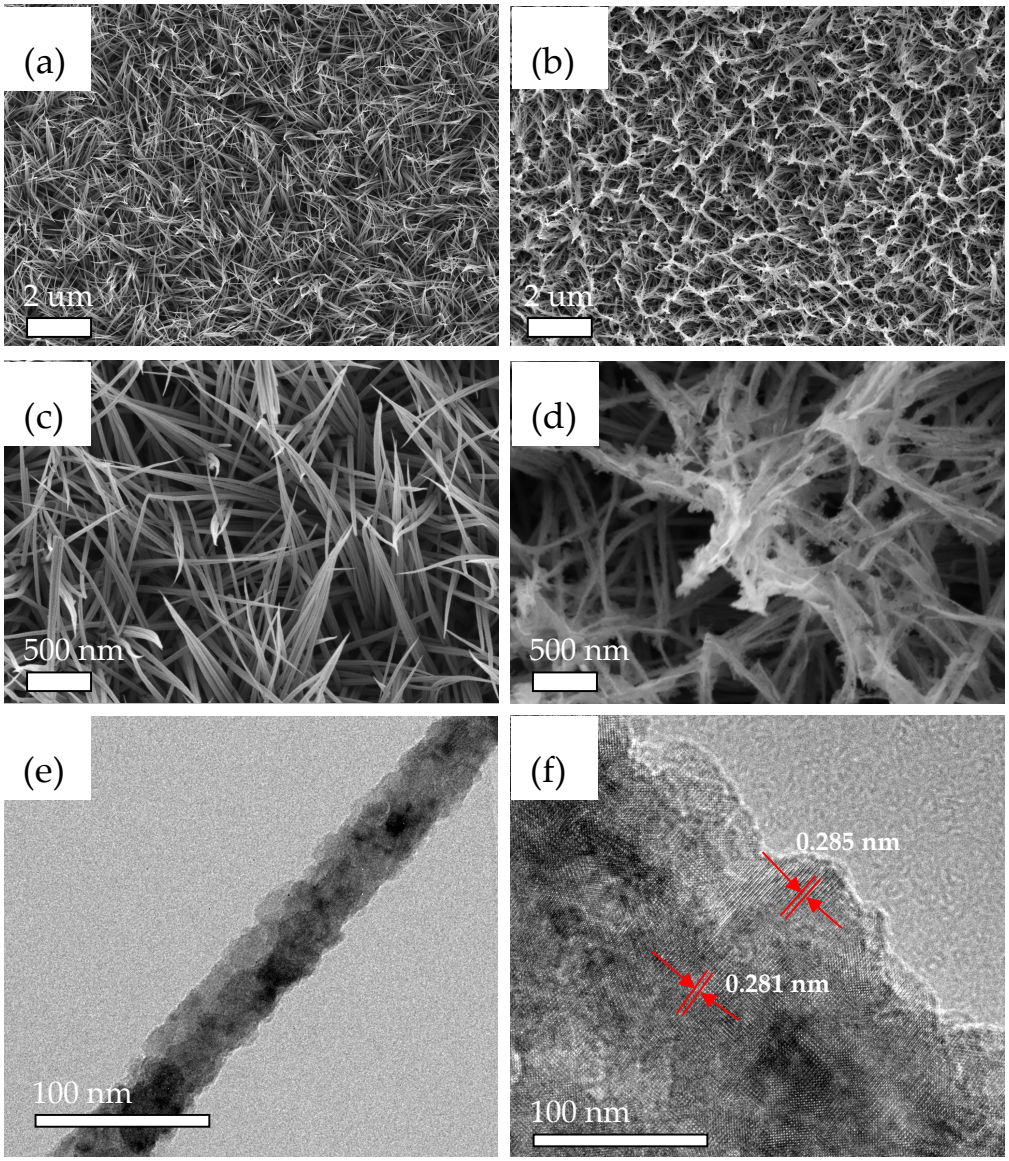

Figure 3. (**a**,**b**) SEM images for $NiCo_2S_4$ samples, (**c**) low magnification SEM images for $NiCo_2S_4$@$NiMoO_4$, (**d**) high-magnification SEM images, (**e**,**f**) TEM images for $NiCo_2S_4$@$NiMoO_4$ samples.

Figure 5a depicts the CV curves of $NiCo_2S_4$@$NiMoO_4$, $NiCo_2S_4$ and $NiMoO_4$ electrodes at 10 mV s^{-1}. It is discovered that the envelope area of the CV curve of the $NiCo_2S_4$@$NiMoO_4$ electrode is larger than that of $NiCo_2S_4$ and $NiMoO_4$ samples, indicating that the $NiCo_2S_4$@$NiMoO_4$ electrode has a large capacitance. The GCD curves of three electrode materials at 1 A g^{-1} are shown in Figure 5b, in which $NiCo_2S_4$@$NiMoO_4$ electrode material has longer discharge time than $NiCo_2S_4$ and $NiMoO_4$ samples, indicating its high specific capacitance. The dynamic characteristics of different electrodes in the frequency range of 100 kHz to 0.01 Hz with an amplitude of 0.01 V are analyzed by electrochemical impedance spectroscopy (EIS), as shown in Figure 5c. In the high-frequency region, the intercept of the real axis corresponds to the equivalent series resistance (Rs), and the radius of the semicircle corresponds to represents the transfer resistance (Rct). In the low-frequency region, the slope of the line is attributed to the Warburg resistance [29]. The lower Rs value of $NiCo_2S_4$@$NiMoO_4$ electrode indicates that it has higher conductivity. The $NiCo_2S_4$@$NiMoO_4$ electrode showed a more vertical line along the imaginary axis, indicating that the ion diffusion process was relatively fast. $NiCo_2S_4$@$NiMoO_4$ electrode

has excellent electrical conductivity. In order to study the cycle stability of three electrode materials, 10,000 cycles of charge–discharge experiments were carried out at 3 A g^{-1} current density, as shown in Figure 5d, indicating that $NiCo_2S_4$@$NiMoO_4$ has good cycle stability with 69% capacitance retention.

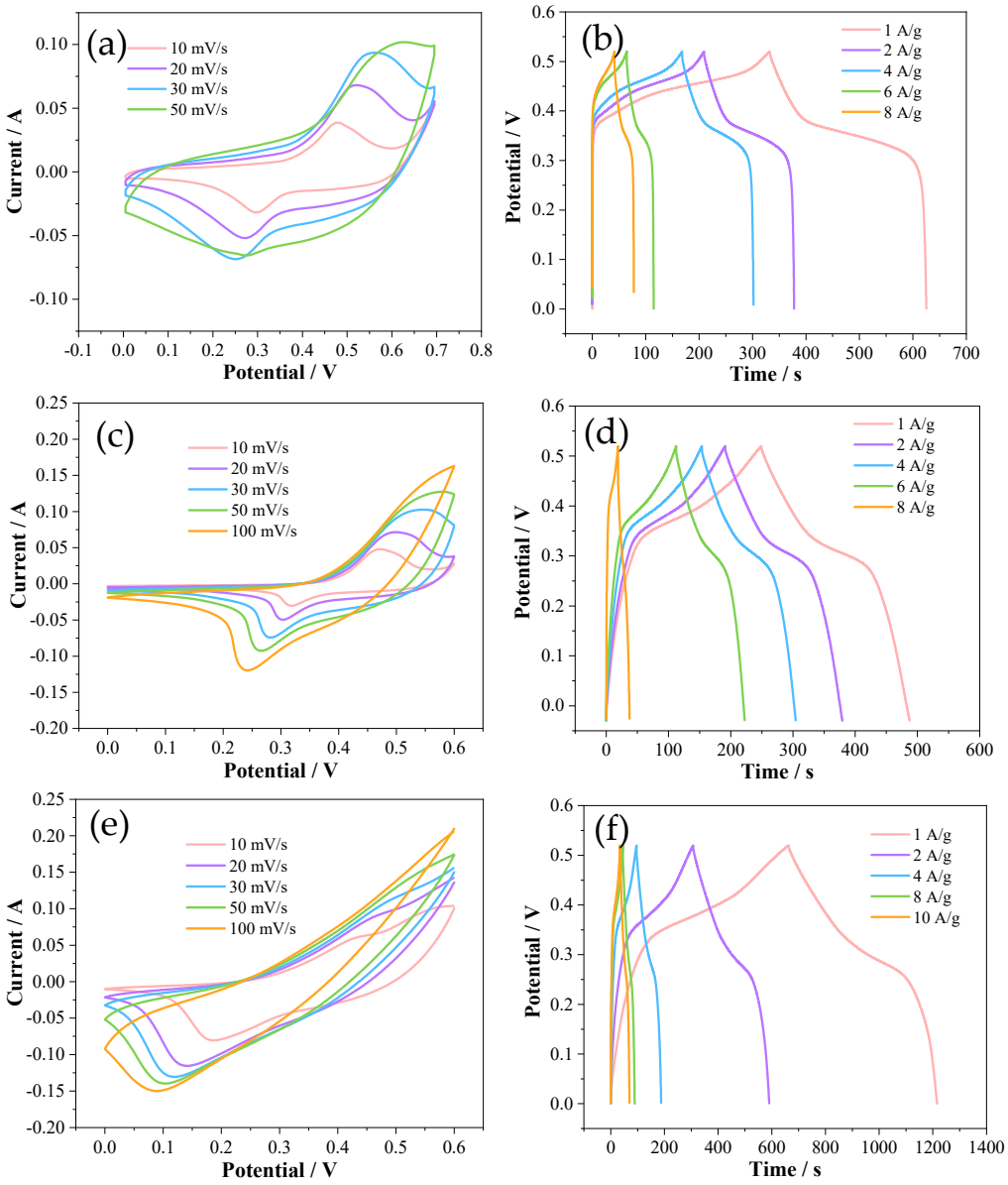

Figure 4. (**a**) CV curves of $NiCo_2S_4$, (**b**) GCD curves of $NiCo_2S_4$, (**c**) CV curves of $NiMoO_4$ samples, (**d**) GCD curves, (**e**) CV curves of $NiCo_2S_4$@$NiMoO_4$ samples, (**f**) GCD curves of $NiCo_2S_4$@$NiMoO_4$ samples.

In order to further explore the practical application of the as-prepared samples, the asymmetric supercapacitor (ASC) was prepared with $NiCo_2S_4$@$NiMoO_4$ as positive electrode and AC as negative electrode. Looking at the CV curves of the device, it is found that the curve area increases with the increase of sweep speed. Figure 6b shows the CV curves of ASC devices under different operating voltage windows. Therefore, the stable voltage windows of the ASC device should be 0–1.6 V. GCD curves of the assembled capacitor under different current densities are shown in Figure 6c. The device delivers a long discharge time of 234.2 s at 1 A g^{-1}. From Figure 6d, it is also confirmed that the device exhibits low resistance. Figure 6e shows the Ragone diagram of $NiCo_2S_4$@$NiMoO_4$//AC ASC. The as-assembled devices possess an energy density of 32.4 W h kg^{-1} at power density

of 3230 W kg^{-1}, reveals that the achieved energy density of our device is distinctly than previously reported capacitive devices [30–34]. Figure 6e shows the cycle stability of the device at 2 A g^{-1}. After 10,000 charge discharge cycles, the capacitance retention of the device reaches 70.1%.

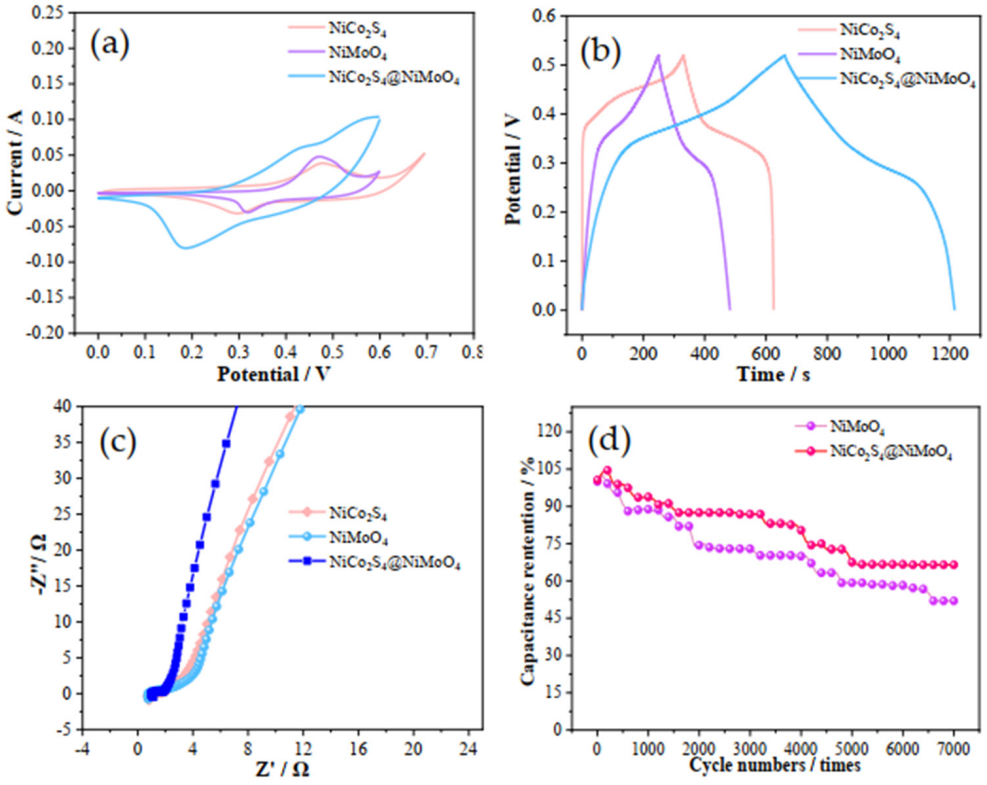

Figure 5. (**a**) Comparison of CV curves of $NiCo_2S_4$@$NiMoO_4$ samples, (**b**) Comparison of GCD curves, (**c**) electrochemical impedance spectroscopy, (**d**) cycle stability.

Finally, the electrochemical performance of the as-prepared samples is also compared with the reported electrode materials, presented in Table 1.

Table 1. Electrocatalytic performance comparison of hybrid structured $NiCo_2S_4$@$NiMoO_4$ with the reported samples.

Material	Capacitance	Current Density	Electrolyte	Ref.
$NiMoO_4$/$CoMoO_4$ clusters	740 F g^{-1}	1.0 A g^{-1}	2 M KOH	[35]
Co_3O4@NiO nanosheet	718 F g^{-1}	2 mA cm^{-2}	3 M KOH	[36]
$CoMoO_4$ nanoparticles	771.6 F g^{-1}	1.0 A g^{-1}	3 M KOH	[37]
$NiMoO_4$ nanorods	680 F g^{-1}	1.0 A g^{-1}	6 M KOH	[38]
$NiCo_2S_4$@$NiMoO_4$	1035 F g^{-1}	1.0 A g^{-1}	3 M KOH	This work

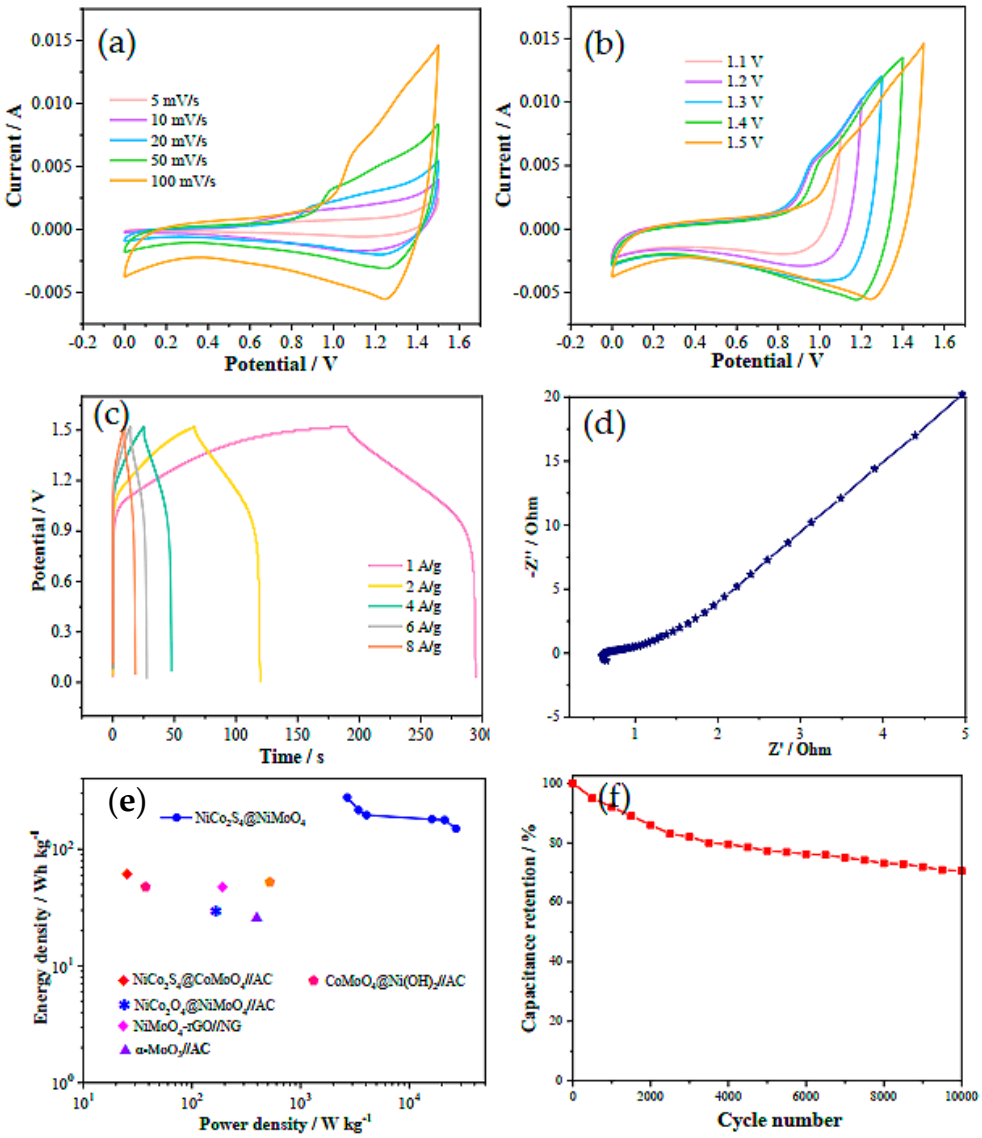

Figure 6. (**a**) CV curves, (**b**) CV curves at different potential, (**c**) GCD curves, (**d**) electrochemical impedance spectroscopy, (**e**) Ragone plot, (**f**) cycle stability.

4. Conclusions

In summary, $NiCo_2S_4$@$NiMoO_4$ electrode material has been successfully synthesized through a simple hydrothermal method. The as-obtained products show high specific capacitance of 1035 F g^{-1} at a current density of 1 A g^{-1}, and excellent cycle stability, which can be ascribed to the unique structure features. Moreover, the as-assembled device shows an outstanding energy density (32.4 W h kg^{-1}), and capacitive retention after 10,000 cycles. This work developed an innovative and simple synthesis method to prepare $NiCo_2S_4$@$NiMoO_4$ electrode materials, and proved the application potential of the prepared $NiCo_2S_4$@$NiMoO_4$ nanosheets structure in energy storage equipment.

Author Contributions: Conceptualization, J.W.; methodology, Y.L.; software, S.S.; validation, J.W. and Y.Z.; formal analysis, J.K.; investigation, J.W.; resources, Y.Z.; data curation, J.W.; writing—original draft preparation, J.W.; writing—review and editing, J.W.; visualization, D.Z. and J.W.; supervision, J.W. All authors have read and agreed to the published version of the manuscript.

Funding: This research was funded by Liaoning Revitalization Talents Program (XLYC1907138), the Natural Science Foundation of Liaoning Province (2019-MS-239, 2020-MS-241), the Scientific Research Fund of Liaoning Provincial Education Department (JL-1901, JL-1903, JL-1916, JL-2021),

the Technology Innovation Talent Fund of Shenyang (RC190360) and Liaoning BaiQianWan Talents Program, the innovation talent fund of Liaoning Province colleges (LR2019046).

Conflicts of Interest: The authors declare no competing financial interest.

References

1. Zhao, D.; Dai, M.; Liu, H.; Duan, Z.; Tan, X.; Wu, X. Bifunctional $ZnCo_2S_4$ hybrid electrocatalysts for high efficient overall water splitting. *J. Energy Chem.* **2022**, *69*, 292–300. [CrossRef]
2. Pang, A.L.; Husin, M.R.; Arsad1, A.; Ahmadipour, M. Effect of graphene nanoplatelets on structural, morphological, thermal, and electri-cal properties of recycled polypropylene/polyaniline nanocomposites. *J. Mater. Sci. Mater. Electron.* **2021**, *32*, 9574–9583. [CrossRef]
3. Ahmadipour, M.; Arjmand, M.; Thirmizir, M.Z.A.; Le, A.T.; Chiam, S.L.; Pung, S.Y. Synthesis of core/shell-structured Ca-Cu3Ti4O12/SiO2 composites for effective degradation of rhodamine B under ultraviolet light. *J. Mater. Sci. Mater. Electron.* **2021**, *32*, 9574–9583.
4. Ahmadipour, M.; Ain, M.F.; Ahmad, Z.A. Effects of annealing temperature on the structural, morphology, optical properties and resistivity of sputtered CCTO thin film. *J. Mater. Sci. Mater. Electron.* **2017**, *28*, 12458–12466. [CrossRef]
5. Chen, X.; Jiang, D.; Li, H.; Xie, K.; Jiang, Y.; Wang, Y. Hydrogen peroxide-induced growth of hierarchical Ni3S2 nanorod/sheet arrays for high performance supercapacitors. *J. Colloid Interface Sci.* **2020**, *575*, 168–176. [CrossRef]
6. Yang, P.; Mai, W. Flexible solid-state electrochemical supercapacitors. *Nano Energy* **2014**, *8*, 274–290. [CrossRef]
7. Wu, X.; Yao, S. Flexible electrode materials based on WO3 nanotube bundles for high performance energy storage devices. *Nano Energy* **2017**, *42*, 143–150. [CrossRef]
8. Wang, X.W.; Sun, Y.C.; Zhang, W.C.; Liu, J.; Wu, X. Hierarchical Cu0.92Co2.08O4@NiCo layered double hydroxide nanoarchitectures for asymmetric flexible energy storage device Mater. *Today Sus.* **2022**, *17*, 100097.
9. Dai, M.Z.; Zhao, D.P.; Wu, X. Research progress on transition metal oxide based electrode materials for asymmetric hybrid capacitors. *Chin. Chem. Lett.* **2020**, *31*, 2177–2188. [CrossRef]
10. Liu, Y.; Hu, P.F.; Liu, H.Q.; Song, J.R.; Umar, A.; Wu, X. Toward a high-performance asymmetric hybrid capacitor by electrode optimization. *Inorg. Chem. Front.* **2019**, *6*, 2824–2831. [CrossRef]
11. Li, B.; Zheng, M.; Xue, H.; Pang, H. High performance electrochemical capacitor materials focusing on nickel based materials. *Inorg. Chem. Front.* **2016**, *3*, 175–202. [CrossRef]
12. Liu, H.Q.; Zhao, D.P.; Hu, P.F.; Chen, K.F.; Wu, X.; Xue, D.F. Design strategies toward achieving high performance Co-MoO4@Co1.62Mo6S8 electrode materials. *Mater. Today Phys.* **2020**, *13*, 100197. [CrossRef]
13. Zhao, D.P.; Zhang, R.; Dai, M.Z.; Liu, H.Q.; Jian, W.; Bai, F.Q.; Wu, X. Constructing high efficient $CoZnxMn_2$-xO_4 electrocatalyst by regulating the electronic structure and surface reconstruction. *Small* **2022**, *18*, 2107268. [CrossRef] [PubMed]
14. Xiong, S.; Lin, M.; Wang, L.; Liu, S.; Weng, S.; Jiang, S.; Xu, Y.; Jiao, Y.; Chen, J. Defects-type three-dimensional Co3O4 nanomaterials for energy conversion and low temperature energy storage. *Appl. Surf. Sci.* **2021**, *546*, 149064. [CrossRef]
15. Liu, Y.; Zhao, D.P.; Liu, H.Q.; Umar, A.; Wu, X. High performance hybrid supercapacitor based on hierarchical MoS2/Ni3S2 metal chalcogenide. *Chin. Chem. Lett.* **2019**, *30*, 1071–1076. [CrossRef]
16. Xie, W.; Xu, Z.; Zheng, W.; Wang, W.; Wang, C.; Zhang, C.; Sun, H. Fabrication of Ni_3S_2 nanoneedle-sheets electrode material with ultrahigh areal capacity of over 15 mAh cm^{-2}. *Mater. Lett.* **2021**, *282*, 128716. [CrossRef]
17. Zhao, D.P.; Dai, M.Z.; Zhao, Y.; Liu, H.Q.; Liu, Y.; Wu, X. Improving electrocatalytic activities of $FeCo_2O_4$@$FeCo_2S_4$@PPy electrodes by surface/interface regulation. *Nano Energy* **2020**, *72*, 104715. [CrossRef]
18. Li, Z.S.; Li, B.L.; Liao, C.N.; Liu, Z.S.; Li, D.H.; Wang, H.Q.; Li, Q.Y. One-pot construction of 3-D graphene nanosheets/Ni_3S_2 nanoparti-cles composite for high-performance supercapacitors. *Electrochim. Acta* **2017**, *253*, 344–356. [CrossRef]
19. Patil, S.J.; Kim, J.H.; Lee, D.W. Self-assembled Ni_3S_2//$CoNi_2S_4$ nanoarrays for ultra-high-performance supercapacitor. *Chem. Eng. J.* **2017**, *322*, 498–509. [CrossRef]
20. Chen, L.; Guan, L.; Tao, J. Morphology control of Ni_3S_2 multiple structures and their effect on supercapacitor performances. *J. Mater. Sci.* **2019**, *54*, 12737–12746. [CrossRef]
21. Liu, H.Q.; Zhao, D.P.; Dai, M.Z.; Zhu, X.F.; Qu, F.Y.; Umar, A.; Wu, X. PEDOT decorated CoNi2S4 nanosheets electrode as bifunctional electrocatalyst for enhanced electrocatalysis. *Chem. Eng. J.* **2022**, *428*, 131183. [CrossRef]
22. Liu, H.; Zhao, D.; Liu, Y.; Tong, Y.; Wu, X.; Shen, G. NiMoCo layered double hydroxides for electrocatalyst and supercapacitor electrode. *Sci. China Mater.* **2021**, *64*, 581–591. [CrossRef]
23. Tian, Z.; Yin, J.; Wang, X.; Wang, Y. Construction of Ni_3S_2 wrapped by rGO on carbon cloth for flexible supercapacitor application. *J. Alloys Compd.* **2019**, *777*, 806–811. [CrossRef]
24. Zhao, R.; Cui, D.; Dai, J.; Xiang, J.; Wu, F. Morphology controllable $NiCo_2O_4$ nanostructure for excellent energy storage device and overall water splitting. *Sustain. Mater. Technol.* **2020**, *24*, e00151. [CrossRef]
25. Gao, Z.; Chen, C.; Chang, J.; Chen, L.; Wang, P.; Wu, D.; Xu, F.; Jiang, K. Porous Co_3S_4@Ni_3S_4 heterostructure arrays electrode with vertical electrons and ions channels for efficient hybrid supercapacitor. *Chem. Eng. J.* **2018**, *343*, 572–582. [CrossRef]

26. Shen, M.; Liu, J.; Liu, T.; Yang, C.; He, Y.; Li, Z.; Li, J.; Qian, D. Oxidant-assisted direct-sulfidization of nickel foam toward a self-supported hierarchical Ni3S2@Ni electrode for asymmetric all-solid-state supercapacitors. *J. Power Sources* **2019**, *448*, 227408. [CrossRef]
27. Liu, C.; Wu, X.; Wang, B. Performance modulation of energy storage devices: A case of Ni-Co-S electrode materials. *Chem. Eng. J.* **2020**, *392*, 123651. [CrossRef]
28. Liu, S.D.; Lee, S.C.; Patil, U.M.; Ray, C.; Sankar, K.V.; Zhang, K.; Kundu, A.; Kang, S.; Park, J.H.; Jun, S.C. Controllable sulfuration engineered NiO nanosheets with enhanced capacitance for high rate supercapacitors. *J. Mater. Chem. A* **2017**, *5*, 4543–4549. [CrossRef]
29. Liu, H.Q.; Dai, M.Z.; Zhao, D.P.; Wu, X.; Wang, B. Realizing superior electrochemical performance for asymmetric capacitors through tailoring electrode architectures. *ACS Appl. Energy Mater.* **2020**, *3*, 7004–7010. [CrossRef]
30. Liu, Y.; Hu, P.F.; Liu, H.Q.; Wu, X.; Zhi, C.Y. Tetragonal VO_2 hollow nanospheres as robust cathode materials for aqueous zinc ion batteries. *Mater. Today Energy* **2020**, *17*, 100431. [CrossRef]
31. Sun, W.; Xiao, L.; Wu, X. Facile synthesis of NiO nanocubes for photocatalysts and supercapacitor electrodes. *J. Colloid Interface Sci.* **2019**, *554*, 705–710. [CrossRef] [PubMed]
32. Wen, S.; Liu, Y.; Zhu, F.; Shao, R.; Xu, W. Hierarchical MoS_2 nanowires/$NiCo_2O_4$ nanosheets supported on Ni foam for high-performance asymmetric supercapacitors. *Appl. Surf. Sci.* **2018**, *428*, 616–622. [CrossRef]
33. Bandyopadhyay, P.; Saeed, G.; Kim, N.H.; Jeong, S.M.; Lee, J.H. Fabrication of hierarchical Zn–Ni–Co–S nanowire arrays and graphitic carbon nitride/graphene for solid-state asymmetric supercapacitors. *Appl. Surf. Sci.* **2021**, *542*, 148564. [CrossRef]
34. Iqbal, M.Z.; Khan, J. Optimization of cobalt-manganese binary sulfide for high performance supercapattery devices. *Electrochim. Acta* **2021**, *368*, 137529. [CrossRef]
35. Wan, H.Z.; Jiang, J.J.; Ji, X.; Miao, L.; Zhang, L.; Xu, K.; Chen, H.C.; Ruan, Y.J. Rapid microwave-assisted synthesis NiMoO4· H2O nanoclusters for supercapacitors. *Mater. Lett.* **2013**, *108*, 164–167. [CrossRef]
36. Bhattarai, R.M.; Pandiyarajan, S.M.S.; Saud, S.; Kim, S.J.; Mok, Y.S. Synergistic effects of nanocarbon spheres sheathed on a binderless CoMoO4 electrode for high-performance asymmetric supercapacitor. *Dalton Trans.* **2020**, *49*, 14506–14519. [CrossRef]
37. Neeraj, N.S.; Mordina, B.; Srivastava, A.K.; Mukhopadhyay, K.; Prasad, N.E. Impact of process conditions on the electrochemical performances of NiMoO4 nanorods and activated carbon based asymmetric supercapacitor. *Appl. Sur. Sci.* **2019**, *473*, 807–819. [CrossRef]
38. Zhang, Y.; Chang, C.R.; Jia, X.D.; Cao, Y.; Yan, J.; Luo, H.W.; Gao, H.L.; Ru, Y.; Mei, H.X.; Zhang, A.Q.; et al. Influence of metallic oxide on the morphology and enhanced supercapacitive performance of NiMoO4 electrode material. *Inorg. Chem. Commun.* **2020**, *112*, 107697. [CrossRef]